Using Joint Time-Frequency Analysis to Analyze Time-Domain Simulations of Shielding Structures

Robert T. Johnk, Bruce Archambeault, and David R. Novotny

Introduction

Simulation of real-world EMC effects has recently become popular. These simulations can be performed in either the frequency-domain (typically, Method of Moments (MoM) and Finite Element Method (FEM)) or in the time-domain (typically, Finite-Difference Time-Domain (FDTD), Transmission Line Matrix method (TLM), or Partial Element Equivalent Circuit (PEEC) method). Simulation in each domain has its advantages and disadvantages. However, time domain simulation is a commonly used EMC tool, mostly due the ease of use of FDTD simulators and the ability to model transient and wideband effects.

Time domain simulation tools are extremely powerful. However, if a structure is resonant with a high Q-factor, the simulations can require long computational times. Classic examples of this effect are encountered in highly resonant structures, such as shielded enclosures and in the decoupling of power/ground planes in printed circuit boards. FDTD is especially useful for modeling these. In the shielded enclosure case, slots and apertures are easily included in the model. In the decoupling example, FDTD easily allows dielectric materials to be included. The main disadvantage of modeling these types of structures with a conventional FDTD analysis (or any other time domain simulation tool) is the long run time required.

Joint Time Frequency Analysis (JTFA) is a powerful tool that is used to post process waveforms obtained from time-domain numerical simulations. JTFA is applied directly to a numerically generated time-domain record, and useful parameters can be extracted using an efficient data processing sequence. The main advantage of JTFA lies in the ability to extract useful parameters using shorter time records. This allows for numerical codes to be run for a shorter length of time, and the final results extrapolated to obtain useful estimates of shielding parameters. This allows more cases to be analyzed and optimal usage of resources by minimizing run-times.

This paper describes the implementation and use of JTFA in conjunction with FDTD simulations of the shielding of slots and enclosures. Several detailed examples are given that highlight the use and application of JTFA.

Joint Time-Frequency Analysis

Joint Time-Frequency Analysis (JTFA) was developed in the 1940's [1,2]. It has reached a high degree of mathematical sophistication and the number of applications continues to grow. Some applications where JTFA has been effectively applied are: processing of speech signals, seismic data processing, image

processing, analysis of musical instruments, and architectural acoustics [3-7]. In the domain of electromagnetics, it has been applied to the analysis of cavities, waveguiding structures, scattering objects, and antennas [8,9]. JTFA also has potential for the investigation of a number of problems in Electromagetic Compatibility (EMC). One EMC application where JTFA shows much promise is the analysis of time-domain numerical simulations of electromagnetic shielding structures, such as metal plates with resonant coupling apertures and metal enclosures with embedded apertures. When these shielding structures are simulated numerically, long run times are often required to compute parameters such as quality factor (Q) and shielding. JTFA provides a nice way to avoid long run times by enabling us, under certain conditions, to extrapolate decay and shielding characteristics beyond the maximum computed time step of a time-domain EM simulation. This allows the engineer to run many more models while varying parameters such as aperture size, etc. We can also use JTFA to gain more insight and information than can be obtained from only a time-domain waveform or its frequency-domain counterpart.

To better understand the JTFA, we start with the traditional Fourier transform defined as [10]:

$$H(f) = \int_{-\infty}^{\infty} h(t)\, e^{-j2\pi ft}\, dt \qquad (1)$$

where f is the frequency (Hz), $h(t)$ is the time-domain waveform to be analyzed, and $H(f)$ is the complex frequency spectrum (magnitude & phase). In practice, we process discrete waveforms generated by time-domain electromagnetic codes. The outputs are finite-duration data sequences $h(t_i)$ of length N, where i = 1,2,3,..,N. We can efficiently analyze the frequency content by applying a Fast-Fourier transform (FFT) to obtain a discrete frequency spectrum $H(f_i)$. The Fourier transform analyzes a signal and provides information about its magnitude and phase across frequency. It does not tell us anything about the time at which a particular frequency component appears in a signal. This is one drawback of the Fourier transform, it does not have any ability to provide resolution in time—the time information is embedded in the phase of the signal and is distributed throughout all of the frequencies. One way to overcome this difficulty is through a multiplication of the signal in (1) by a windowing function to yield:

$$G(f,\tau) = \int_{-\infty}^{\infty} g(t)\, w(t-\tau)\, e^{-j2\pi ft}\, dt \qquad (2)$$

where $G(f,\tau)$ is the short-time Fourier transform (STFT) [2], $w(t)$ is a specified windowing function over the time interval, 0≤ t ≤W, and is zero elsewhere. The parameter τ is the amount by which the window is shifted in time to analyze a selected section of the waveform $h(t)$. The short-time Fourier transform is a function of two variables, time (τ) and frequency (f), and hence term "Joint Time-Frequency Analysis." With JTFA we now analyze both the frequency content of a waveform and the time interval during which a frequency component is generated. The process of performing a JTFA analysis is one of sliding a window over a time-domain signal and Fourier analyzing it at a succession of window positions. Smaller window widths provide better resolution in time, and wider windows less resolution in time. There is a tradeoff, however. The ability to resolve signals

simultaneously in both the time and frequency domains can be precisely stated in terms of the so-called uncertainty relation [11]:

$$\Delta t \Delta f \geq \frac{1}{2\pi} \qquad (3)$$

where Δt is the time resolution (sec) and Δf is the frequency resolution Hz. Thus our ability to resolve simultaneously in both time and frequency is limited. If we desire high resolution in frequency, we must accept less in the time domain. Conversely, if we desire more resolution in time we must accept less in the frequency domain.

Table 1. Some commonly used windows suitable for short-time Fourier analysis.

Window Type	Functional Form (i=0,1,…N-1)
Rectangular	w(i)=1
Hanning	$w(i) = 0.5 - 0.5 \cos(2\pi i/N)$
Blackman	$w(i)=0.42-0.5 \cos(2\pi i/N)-0.08 \cos(4\pi i/N)$
Hamming	$w(i) = 0.54 - 0.46 \cos(2\pi i/N)$
Kaiser-Bessel	$w(i)=I_0(\beta[1.0-a^2])/ I_0(\beta)$ where I_0 is the zero-order modified Bessel function, a=(i-k)/k, k=(N-1)/2

Windowing

Windowing is simply a process of isolating a desired section of a waveform and deleting the rest. There are a number of ways the data within the window can be treated. One approach is to leave the data unaltered using a rectangular window. An example of a rectangular window is illustrated in Figure 1 in which a 40ns wide window is applied to a waveform. Alternatively, we can taper the signal using a number of possible window types. Some well-known tapered windows are: Hanning, Hamming, Blackman, and Kaiser-Bessel, summarized in Table 1. A more extensive summary of available window types and mathematical properties is provided in [12]. Again, there are trade-offs when deciding which window function to use. Figure 2a depicts the time- and frequency-domain properties of several commonly used windows. In the case of the rectangular window, an abrupt truncation in the time-domain leads to a frequency-domain amplitude spectrum that has a narrow main lobe characteristic; first and second sidelobe levels at -13 dB and -17 dB respectively. When the Hanning taper of Figure 2b is applied, the width of the main lobe is nearly twice that of a rectangular window, however the first sidelobe level drops down to -37 dB. In general, tapering increases the width of the main lobe and reduces the level of the sidelobes, which increases the dynamic range of the frequency domain result. An extremely useful window for this type of analysis is the Kaiser-Bessel window. This window function has a variable index β which allows for a wide range of taper characteristics. This feature makes the Kaiser-Bessel window ideal for JTFA. Figures 2c and 2d depict

Kaiser Bessel window characteristics for indices of 1.0 and 1.6 respectively. For β=1.0, the main lobe is only somewhat wider than that of the rectangular window, and it has lower sidelobe levels—a significant improvement over the rectangular window. Setting β=1.6 obtains characteristics that are slightly better than those of the Hanning window.

In order to understand the impact of windowing in JTFA, consider the following complex waveform consisting of a number of sinusoids damped by differing amounts:

$$s(t) = 0.1\sin(2\pi f_1 t) + Exp[-d_1 t]\sin(2\pi f_2 t) + Exp[-d_2 t]\sin(2\pi f_3 t) + Exp[-d_3 t]\sin(2\pi f_4 t) \quad (4)$$

where f_i (i=1,2,3,4) are the frequencies of the sinusoidal waveforms, and d_i (i=1,2,3) are exponential decay rates. One possible waveform is plotted in Figures 3a, along with the frequency-domain amplitude spectrum in Figure 3b. This waveform has frequency components at 200, 500, 800, and 1100 MHz, with decay rates d_1=5x10^6, d_2=15x10^6, and d_3=50x10^6. The waveform has a very complex structure and resembles those encountered in time domain shielding simulations. The simple FFT frequency-domain plot clearly separates the four components with progressively lower Q-factors as the frequency increases. Neither the time- nor the frequency-domain plots clearly highlight the decay rates.

The power of JTFA can be applied to this waveform. Figure 4 shows the results of a JTFA analysis using three different 100ns duration window types. We now have a 3-dimensional graph with spectrum amplitude plotted as a function of time and frequency. The frequency components appear as ridges which are parallel to the τ-, or time, axis. The amount of definition (dynamic range) achieved depends on the window used. A rectangular window is used in Figure 4a, and the "valleys" between the ridges are filled in by high sidelobe levels. Application of a Hanning window improves the dynamic range and produces much better definition as is seen in Figure 4b. This is particularly the case with the 1100 MHz component which is barely visible in the rectangular window analysis, and becomes well defined upon application of a tapered window. Better results were obtained with a Kaiser-Bessel window (index β=3.0) and is shown in Figure 4c. Not only are the frequency components visible with deep "valleys" in between, but the varying rates of decay are clearly visible. The decay rates are proportional to the downward rates of descent of the ridge peaks. The capability to display and analyze decay rates directly is a powerful feature of JTFA in the analysis of shielding problems.

JTFA of a Resonant Slot in a Metal Sheet – a Canonical Example

We now consider the analysis of a resonant slot embedded in an infinite metal sheet using the Finite-Difference Time-Domain (FDTD) technique [13]. The geometry is shown in Figure 5a, and consists of a pulsed current source, a perfectly-conducting metal sheet that extends out to the edge of the computational domain (simulating a sheet of infinite extent), a 30.0 cm x 0.1cm slot, and an ideal

field monitor point, located 6.0 m from the slot center provides information on the three electric-field components. The source is an impressed electric current density that is rapidly switched on and off, generating a pulsed electromagnetic wave traveling outward in all directions at the speed of light. The source approximates a short radiating dipole (1.0 cm long) having broad directional coverage. A portion of the wavefront penetrates to the other side of the sheet. A monitor point, located at a specified location on the other side of the sheet, measures the component fields 6.0 m away from the center of the slot. One way to quantify the amount of slot penetration is to compare the results with the free-space geometry of Figure 5b, where the metal sheet/slot combination has been removed. The free-space configuration provides a reference for comparison and allows the results to be normalized to the free-space case. Typical reference and slot waveforms obtained from a FDTD code are shown in Figures 6a and 6b respectively. The reference FDTD waveform has a short temporal extent of approximately 2 ns, and has useable spectrum extending from 100 MHz to approximately 3 GHz. The slot waveform has reduced peak amplitudes, and has an extended time domain response. It has a more complex structure with harmonically-related sinusoidal components that decay exponentially. These components are visible as sharp peaks in the amplitude spectrum at 483, 1483, and 2445 MHz.

The results can be displayed either as “shielding” or “penetration”. High penetration implies low shielding, and conversely, low penetration corresponds to high shielding levels. As we shall see, using penetration instead of shielding generates useful graphical displays. Figure 7 shows the penetration through the slot. The slot exhibits resonant peaks in penetration at a fundamental frequency of 483 MHz and at the third and fifth harmonics of 1483 MHz, and 2445 MHz. A maximum penetration of -9.7 dB (9.7 dB of shielding) occurs at the fundamental slot resonance of 483 MHz at which the slot length is close to one-half wavelength.

If we perform a JTFA analysis on the slot-penetration, time-domain waveform and normalize the results with the amplitude-spectrum of the free-space reference, we effectively remove the frequency dependence of the source. The result is a function of frequency and the window parameters (delay, length, and type), and is more complex. JTFA results obtained for different window lengths are shown in Figures 8a-c. In Figure 8a, a 20ns duration Kaiser-Bessel window (β=3.0) is used. The three resonances are visible as prominent ridges running parallel to the time (τ) axis. The impact of reducing the window length by factors of 2 and 4, (leaving the other parameters unchanged) is shown in Figures 8b and 8c respectively. As the window length decreases, the ridges become broader in frequency. This is a result of the uncertainty principle of time and frequency stated earlier in (3).

We can derive additional information from the JTFA analysis that was not available in the original frequency domain analysis. The amplitudes of the ridges decrease in time (τ), and this is caused by decaying slot resonances. We can extract this decay from the JTFA plot of Figure 8b and obtain the results of Figure 9. The linear characteristic (on a dB scale) indicates an exponential decay. The dashed lines on the plot are the result of a least-squares fit to a straight line. This

procedure directly yields the decay slopes. The fundamental mode exhibits the slowest decay rate, while increasing rates of decay are noted for the third and fifth harmonics. These decay rates can be directly related to the quality factor (Q) through the relation [8]

$$Q = 2\pi\, 10^{-9}\, f\, t_{decay} \tag{5}$$

where f is the frequency (Hz) and t_{decay} is the decay time (ns) of a selected resonance. The decay time is the time it takes for the signal energy to decay to $1/e$ (-4.3 dB) of its original value. Once the slope of the decay is known, the decay time is computed from the formula

$$t_{decay} = \frac{-4.3}{a} \tag{6}$$

Table 2. Q-factors obtained from a JTFA analysis of normalized penetration data. The selected frequencies correspond to slot resonant peaks.

Frequency (MHz)	t_{decay} (ns)	Q-Factor
483	2.90	8.80
1483	1.82	16.95
2445	1.56	23.97

where a is the slope (dB/s) determined by a least-squares fit, and t_{decay} is the decay time (ns). Table 2 below summarizes the Q-factor results obtained directly from the JTFA analysis.

JTFA of a Box with an Embedded Slot Aperture – a Real-World Example

While the analysis of a simple (infinite) metal plate with an aperture is instructive, a complex, real-world analysis is performed on a structure used to study the penetration of electromagnetic signals into aircraft structures, and to develop practical and efficient test procedures to assess aircraft shielding [14]. A shielded enclosure with the previously studied aperture is analyzed. Once a shielded enclosure is added, we would expect to find many more resonant frequencies due to the physical dimensions of the enclosure. Figure 10 shows such a structure. It consists of the same 30 cm x 0.1cm slot embedded in the face of a rectangular metal box with dimensions 1.03 m x 0.93 m x 73 m. The interior of the box contains a metal paddle to function as a diffuser and to maximize excitation of available cavity modes inside the box, and can well simulate obstructions in the box such as a card in a PC or a bulkhead in an aircraft. Two of the box walls are covered with 1cm-thick, lossy dielectric (non-magnetic) walls with the parameters ε_r=1.0, and conductivity, σ, which can be selected to control the rate of decay of the generated waveform. The same pulsed source is located inside the box, and an ideal monitor point is located 6.0 m from the geometric center of the slot. The resulting electric field waveform and the associated penetration spectrum, computed using the same reference waveform as in Figure 6, are shown in Figure 11 with slab conductivities set at σ = 250 S/m. Due to the addition of the box, the

resulting waveform is much more complex, and has a much longer temporal extent than encountered with the slot alone. The penetration spectrum now exhibits a highly complex noise-like spectrum that exhibits large and rapid variations as a function of frequency. Peaks in the penetration spectrum are seen in the vicinity of the slot resonances. This complex structure is due to the modal structure in the box that changes rapidly with frequency, and thereby randomizes the field structure. This is in stark contrast to the isolated slot, for which the variations are better behaved.

If a JTFA is now performed on the box waveform, we obtain the results of Figure 12a. Additional complexity occurs in the multitude of ridges that are caused by the box cavity modes. While the penetration decays with increasing τ, the decay is not distinctly exponential—the behavior is quite erratic. The slot resonances are somewhat visible as broad ridges in the vicinity of the three resonant frequencies. The decay characteristics of several frequency components near the slot resonance peaks are shown in Figure 12b. The decay of the third and fifth overtones is quite erratic, and is clearly not exponential. A complex modulation is imposed, which is caused by interference from additional box modes that are close to the selected frequencies. A similar modulation effect is encountered in the evaluation of the sound properties of rooms in architectural acoustics [7]. We are now dealing with a two-fold complexity in both frequency and time.

In order to obtain meaningful data from this simulation, statistical averaging of the data was performed to smooth out the rapid variations. An efficient way to accomplish this is to frequency average the penetration data over a specified bandwidth [14]. This is implemented by averaging signal energy to obtain a specified bandwidth to obtain the mean penetration

$$\left\langle P(f_n)\right\rangle = \frac{1}{2N+1}\sqrt{\sum_{i=n-N}^{i=n+N} |P(f_i)|^2} \qquad (7)$$

where the index n is the center frequency of the averaging window, N is the number of discrete FFT frequencies above and below the center frequency of the window, and $P(f_i)$ is the penetration at a selected frequency. Equation (7) is equivalent to a rectangular sliding window of width $2N+1$ that performs a smoothing operation by averaging out random variations in the data. The impact of this can be seen in Figures 13a-c where the averaging bandwidth are 10,50, and 200 MHz respectively. Larger frequency bandwidths produce a higher degree of smoothing. As bandwidth increases, the rapid and random variations caused by the box modes are suppressed, highlighting the systematic effects of the slot.

We can use this averaging process in conjunction JTFA results in which we now apply (7) at each window position. The averaged JFTA results are shown in Figure 14 for averaging bandwidths of 50, 100, and 200 MHz. As the averaging bandwidth is progressively increased, the randomizing effects of the box cavity modes are suppressed, and the slot resonances become distinctly visible.

Extracting the decay rate at the three resonant peaks, results in Figure 15a-c. As the averaging bandwidth increases, the decay approaches a single-exponential characteristic (a straight line in dB), and the modulation effect is mitigated. We can now, as earlier, perform a least-squares fit at the three frequencies to obtain the decay characteristics. The results of the fitting process are plotted as dashed lines in the plots. Rapid convergence in decay times occurs with increasing bandwidth, with maximum change of less than 4% in slope noted as bandwidth increases from 100 to 200 MHz. Using equation (5) and (6), we can use the curve fits to estimate Q-factors at the three frequencies, summarized in Table 3. The addition of the box increases the resulting Q-factors by two orders of magnitude. Also, the box/slot interaction shifts the peak resonant frequencies somewhat from those of an isolated slot.

A Proposed Method for Estimating Total Penetration

An FDTD simulation was performed on the box structure of Figure 16 with the same dimensions, ideal monitor point, and the same excitation source as analyzed in the last section. The lossy slabs are no longer present, and each of the six faces has five randomly placed 4 cm x 4 cm square apertures, which do not exhibit any resonant behavior in the 200-3000 MHz frequency range for which the analysis is conducted. Moreover, since the box walls are perfect electric conductors, coupling through the apertures provides the only loss mechanism. The electric field waveform is shown in Figure 17. Ten days on a 1.8 GHz Pentium processor were required to run this simulation for 950ns, and no apparent decay is visible! Clearly, the sub-resonant apertures do not provide much loading! In order to accurately estimate shielding, a much longer run time would be required to achieve a suitable amount of decay in the waveform—this is not a viable option.

Table 3. Energy decay times and associated Q-factors obtained from a JTFA analysis of the box/slot combination of figure. The selected frequencies correspond to slot resonances. The conductance of the dielectric slabs is σ=250 S/m

Frequency (MHz)	t_{decay} (ns)	Q-Factor
502	100	315
1485	115	1,069
2431	149	2,271

Table 4. Energy decay times and associated Q-factors at selected frequencies obtained from a JTFA analysis of the box/slot combination of figure 15. Note how the Q-factors decrease rapidly with increasing frequency.

Frequency (MHz)	t_{decay} (ns)	Q-Factor
1000	3,159	19,850
2000	1,098	13,802
2500	341	5,353
3000	210	3,966

A JTFA analysis using a 200ns Kaiser-Bessel window (β=2.0) on the box waveform and 200 MHz of frequency averaging is shown in Figure 18. Results are shown for several frequencies for which higher rates of decay occur as the frequency is increased. This is a direct consequence of the frequency dependence of the aperture radiated power. Once again, JTFA reveals physical effects that are not visible in the time domain alone. The least-squares fits are shown as dashed lines, and the decay rates are approximately exponential. The resulting Q-factors are summarized in Table 4 below, with considerably higher values than those encountered in the loaded box cases.

The high Q-factors and associated slow decay rates pose a challenge in estimating the penetration. A promising approach that is currently being investigated is first to invoke the assumption of single exponential decay and then extrapolate beyond the computed time range. The process is illustrated in Figure 19. We start with the least-squares fit obtained from a combination of joint time-frequency analysis and frequency averaging. The penetration line is sampled at an interval of W, corresponding to the window width used in the JTFA. The samples give us information about signal energies at sequential and non-overlapping window positions. We can now sum these components to obtain the total penetration. Although there are an infinite number of samples, the assumption of exponential decay results in a simple geometric progression that is readily summed in closed form [15]. Some results obtained, using this method for the configuration of Figure 16 are summarized on Table 5. The penetration increases rapidly above 1000 MHz due to the increasing electrical size of the rectangular apertures. The influences of window function and duration on the structure penetration are currently being investigated. In addition, our research is focusing on the development of guidelines for optimal window parameter selection. The application of this technique to shielding structures is work in progress, and more research is currently being conducted to bring it to maturity.

Conclusions

Table 5. Box penetration computed from a combination of joint time-frequency analysis and a 200 MHz averaging bandwidth

Frequency (MHz)	Penetration (dB) Kaiser-Bessel Window β=2.0, W=200ns
1000	-17.8
2000	-5.1
2500	-6.2
3000	-4.9

Joint time-frequency analysis is a potentially powerful tool for the analysis of EMC shielding problems using time-domain numerical codes. It permits us to use shorter run times, and extract useful parameters such as a Q-factor, and under certain conditions, shielding. The application of this technique to other types of shielding structures is work in progress, and other potential applications of this method are currently being investigated.

Acknowledgements

First and foremost, the authors are deeply indebted to Arthur Ondrejka (NIST Emeritus) for his pioneering work and mentorship in joint time-frequency analysis. We are also indebted to Dave Walen, Tony Wilson, and John Dimtroff of the FAA for their generous support in the development of this powerful tool during 2001-2003. The authors are also indebted to Mike Hatfield of the Naval Surface Warfare Center for his support of the genesis of this technique during 1993-1994. We are also indebted to Perry Wilson and Dennis Friday of the NIST RF Technology division for their generous support.

References

[1] D. Gabor, "Theory of communication," J. IEE (London), vol. 93, pp. 429-457, 1946.

[2] L. Cohen, "Time-frequency distributions-a review," Proc. IEEE, vol. 77, no. 7, July 1989

[3] T.F. Quatieri, *Discrete-Time Speech Signal Processing,* Upper Saddle River N.J.: Prentice-Hall, 2002.

[4] B. B. Hubbard, *The World According to Wavelets*, Natick, MA: A. K. Peters Ltd., 1998.

[5] S. Qian and D. Chen, *Joint Time-Frequency Analysis,* Upper Saddle River N.J.: Prentice-Hall, 1996.

[6] J.F. Alm and J.S. Walker, "Time-frequency analysis of musical instruments," SIAM Review, vol. 44, pp. 457-476, August, 2002.

[7] F. A. Everest, *Master Handbook of Acoustics,* New York, NY: McGraw Hill, 2001.

[8] J..M. Ladbury, R.T. Johnk, A.R. Ondrejka, "Rapid evaluation of mode-stirred chambers using impulsive waveforms, NIST Technical Note 1381, June 1996.

[9] L. Carin and L.B. Felsen, "Wave-oriented data processing for frequency- and time-domain scattering by nonuniform truncated arrays. IEEE Antennas Propagation Magazine, 36: pp. 29-43, 1994.

[10] R. N. Bracewell, *The Fourier Transform and its Applications,* New York, NY: McGraw-Hill, 1978.

[11] L. Cohen, *Time-Frequency Analysis,* Upper Saddle River N.J.: Prentice-Hall, 1995.

[12] A. D. Poularikas, *Handbook of Formulas and Tables for Signal Processing,* Boca Raton, FL: CRC Press, 1999.

[13] A. Taflove and S. Hagness, *Computational Electrodynamics: The Finite-Difference Time-Domain Method,* Boston MA: Artech House, 2000.

[14] C. A. Grosvenor, R. T. Johnk, D. R. Novotny, N. Canales, C. .M. Weil, J. Veneman, *A Two-Phase Airframe Shielding* Performance *Study Using Ultra-wideband Measurement Systems***,** NIST IR, *to be published.*

[15] H. B. Dwight, *Tables of Integrals and Other Mathematical Data,* New York, NY: MacMillan, 1961.

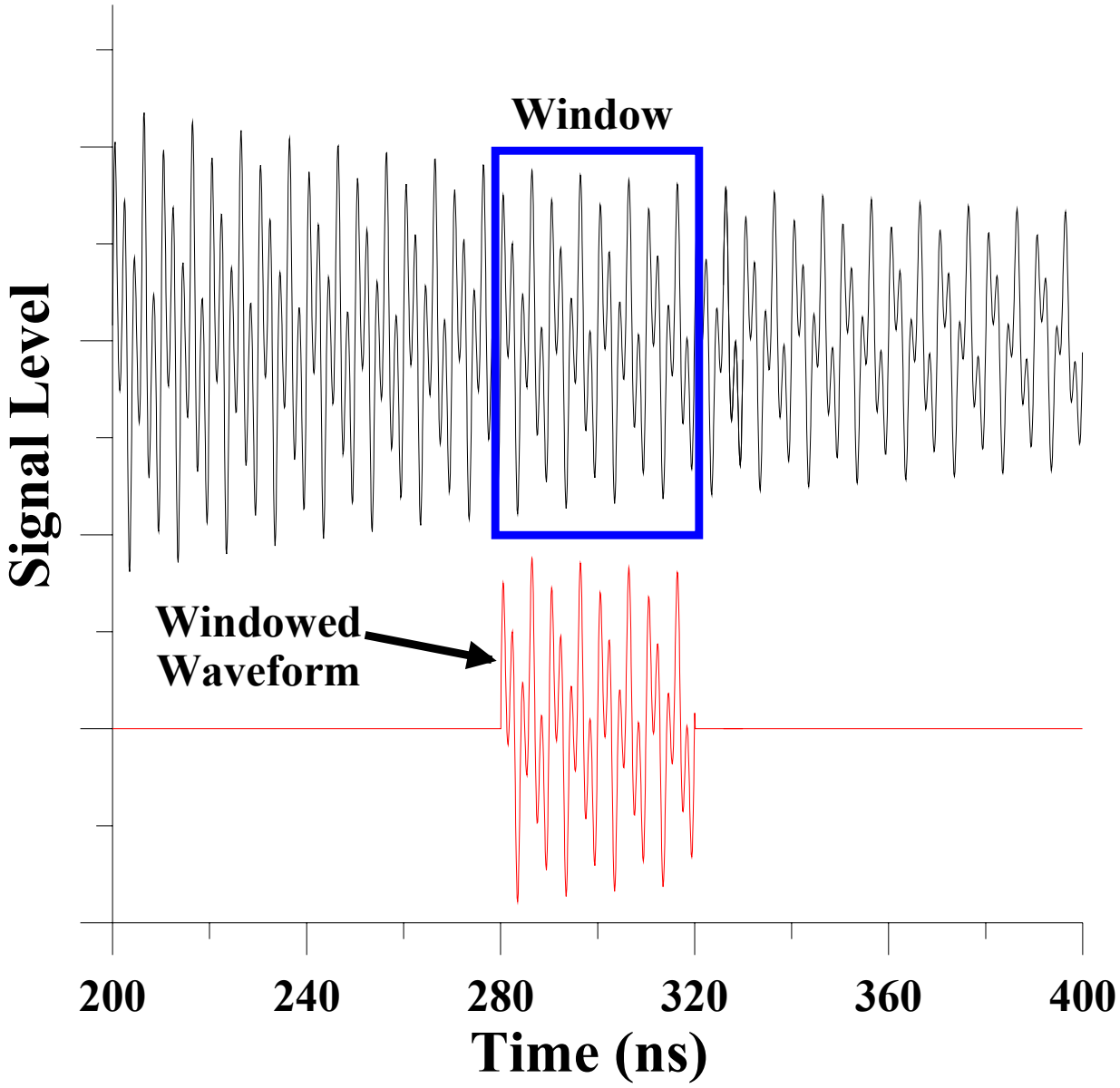

Figure 1. The most basic form of time windowing (rectangular window). The selected section of the top waveform remains unmodified, while the remaining section is deleted.

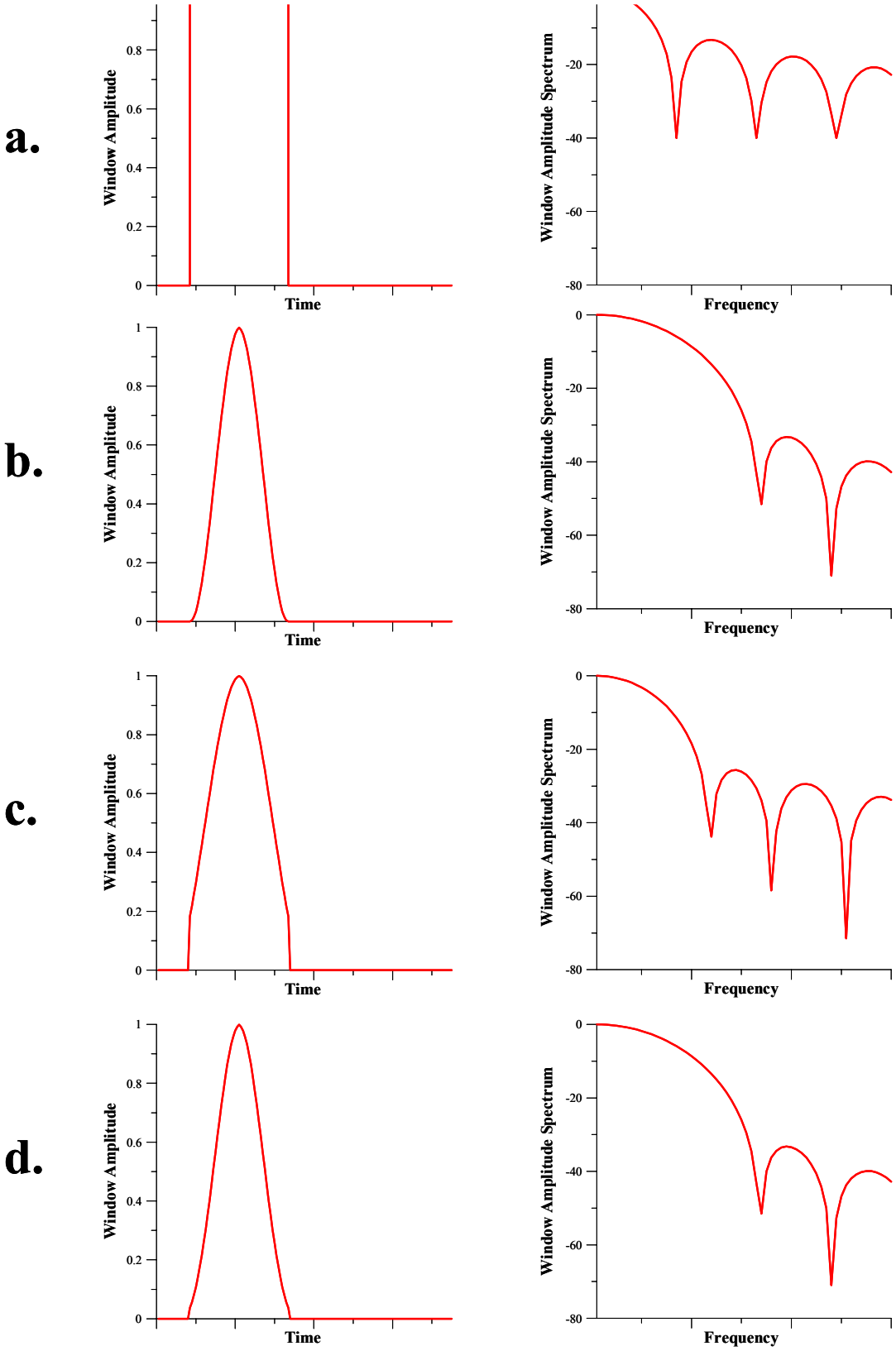

Figure 2. The time and frequency characteristics of four different time windows: **a.** rectangular window, **b.** Hanning window, **c.** Kaiser-Bessel window with index β=1.0, **d.** Kaiser-Bessel window with β=1.6. Note the tradeoffs in the time- and frequency-domains.

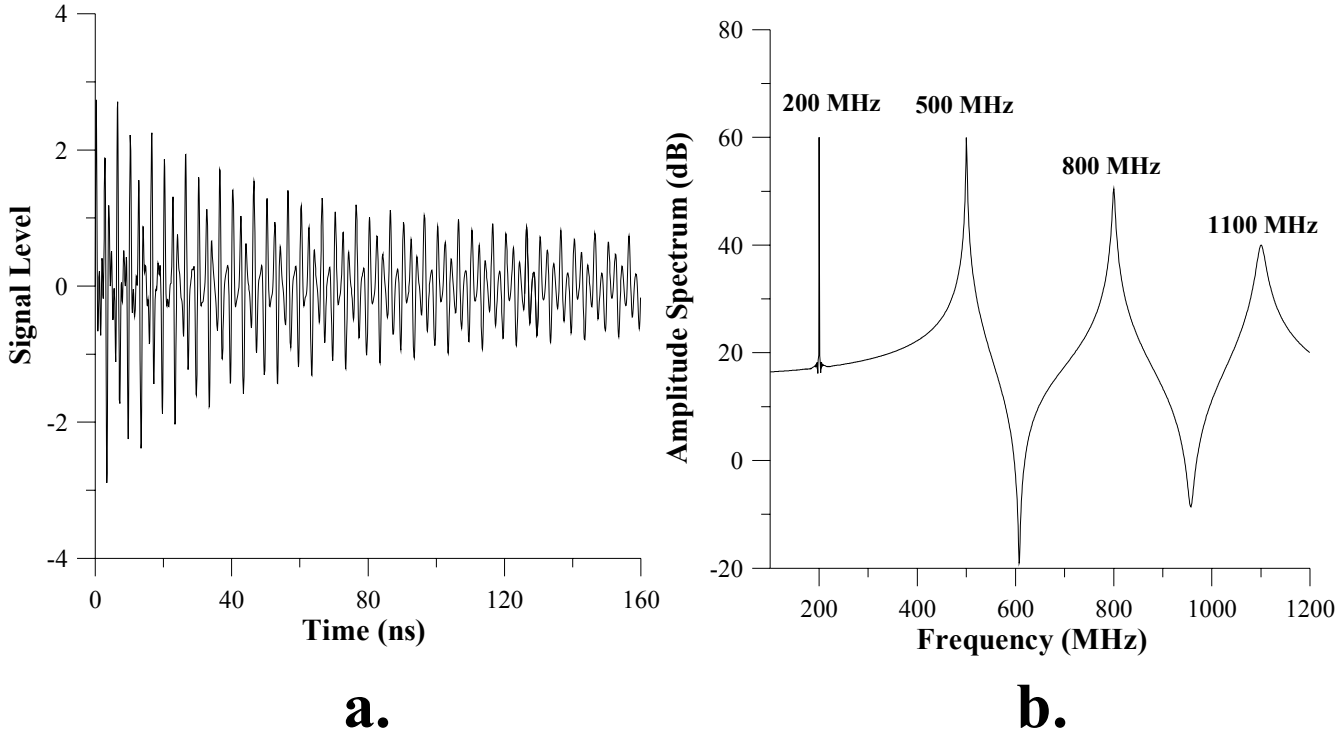

Figure 3 **a.** Waveform obtained from (3) with f_1=200 MHz, f_2=500 MHz, f_3=800 MHz, f_4=1,100 MHz, $d_1=5.0x10^6$, $d_2=5.0x10^6$, and $d_3=1.5\ x10^6$, **b.** Associated amplitude spectrum (the narrow spike at 200 MHz is a result of no decay).

a.

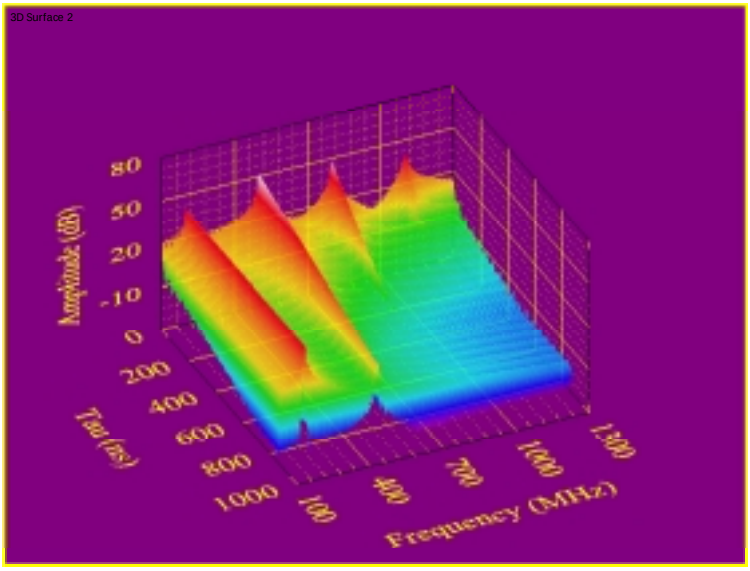

b.

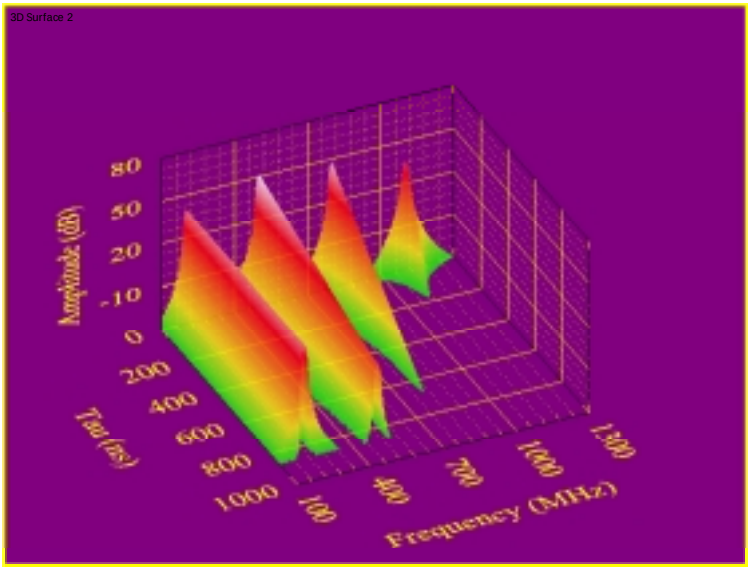

c.

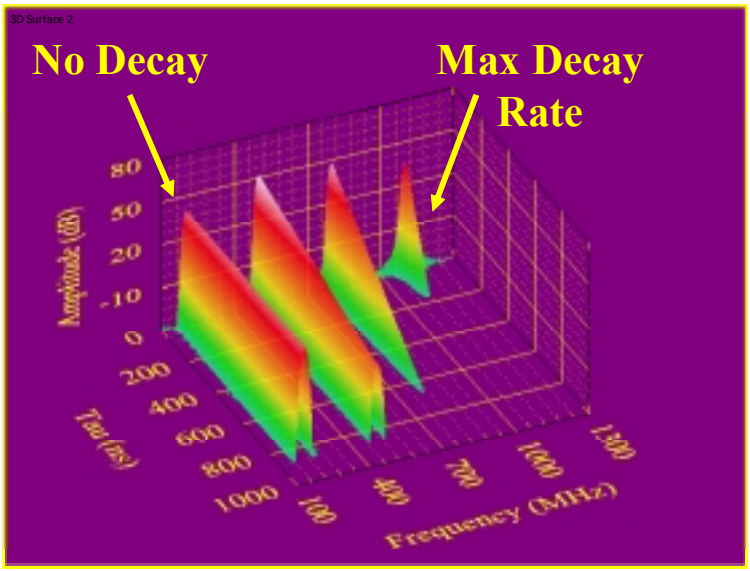

Figure 4. Joint time-frequency analysis of the waveform of (4) using a 100 ns window: **a.** rectangular window, **b.** Hanning window, **c.** Kaiser-Bessel window with β=3.0. Note that the frequency component at 200 MHz does not decay, while increasing decay rates along the time (tau) axis are noted at the higher frequencies.

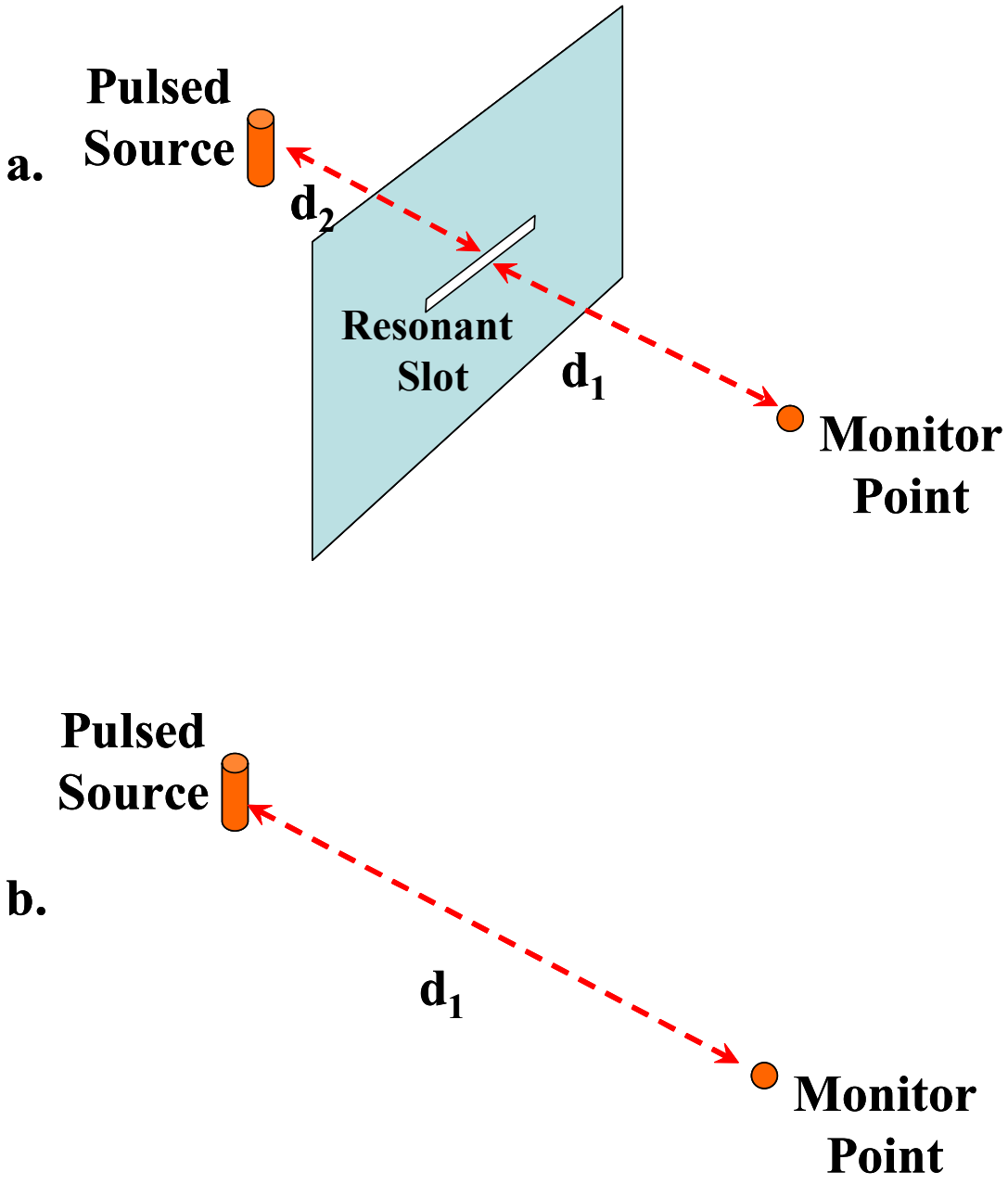

Figure 5 **a.** FDTD model of resonant slot (30.0 cm x 0.1 cm) embedded in a perfectly conducting plane of infinite extent, **b.** FDTD model of free-space reference. d_1=6.0 m and d_2=0.5 m.

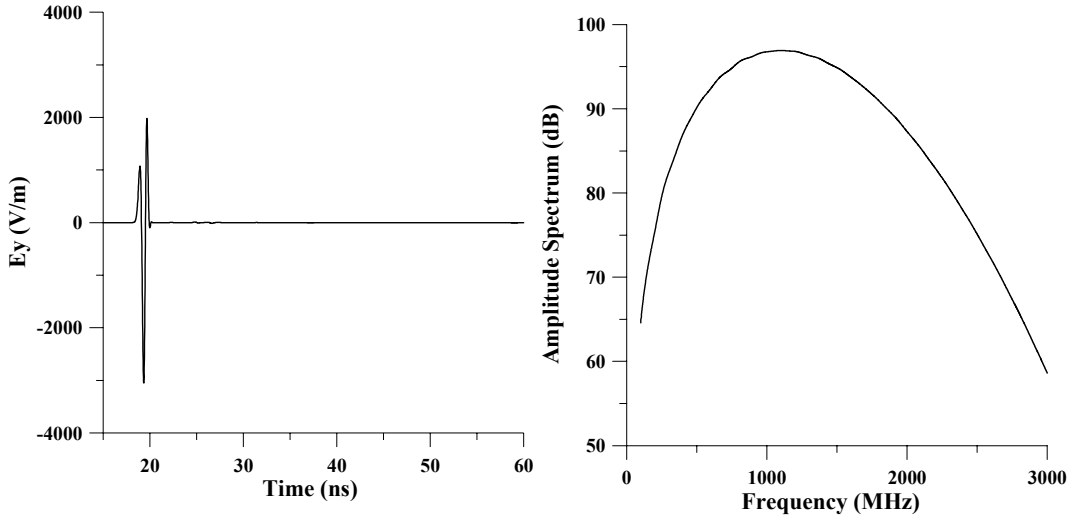

a.

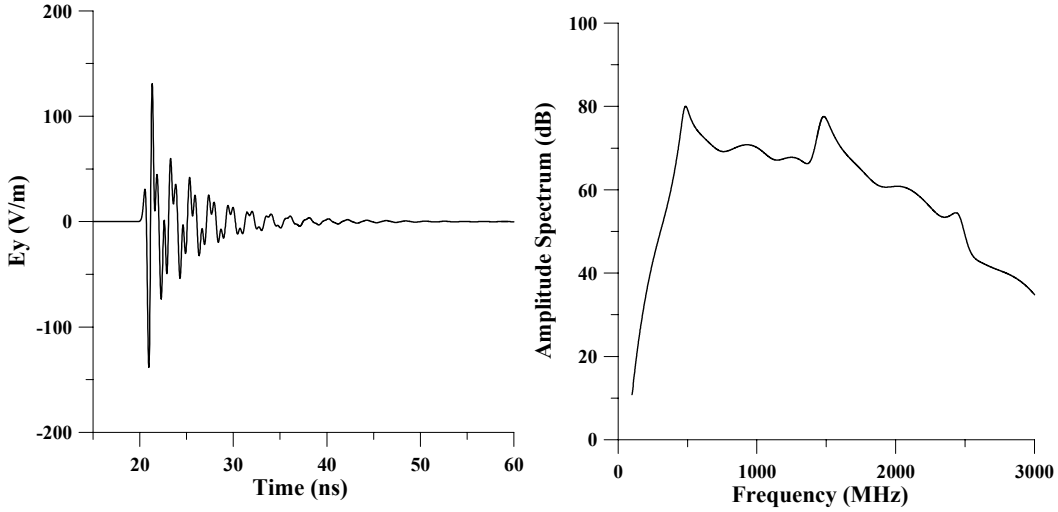

b.

Figure 6 **a.** FDTD generated reference waveform and associated amplitude spectrum, **b.** Waveform and corresponding amplitude spectrum obtained with a 30 cm x 0.1 cm resonant slot embedded in an infinite ground plane. Note the resonant peaks the neighborhood of 500, 1500, and 2500 MHz.

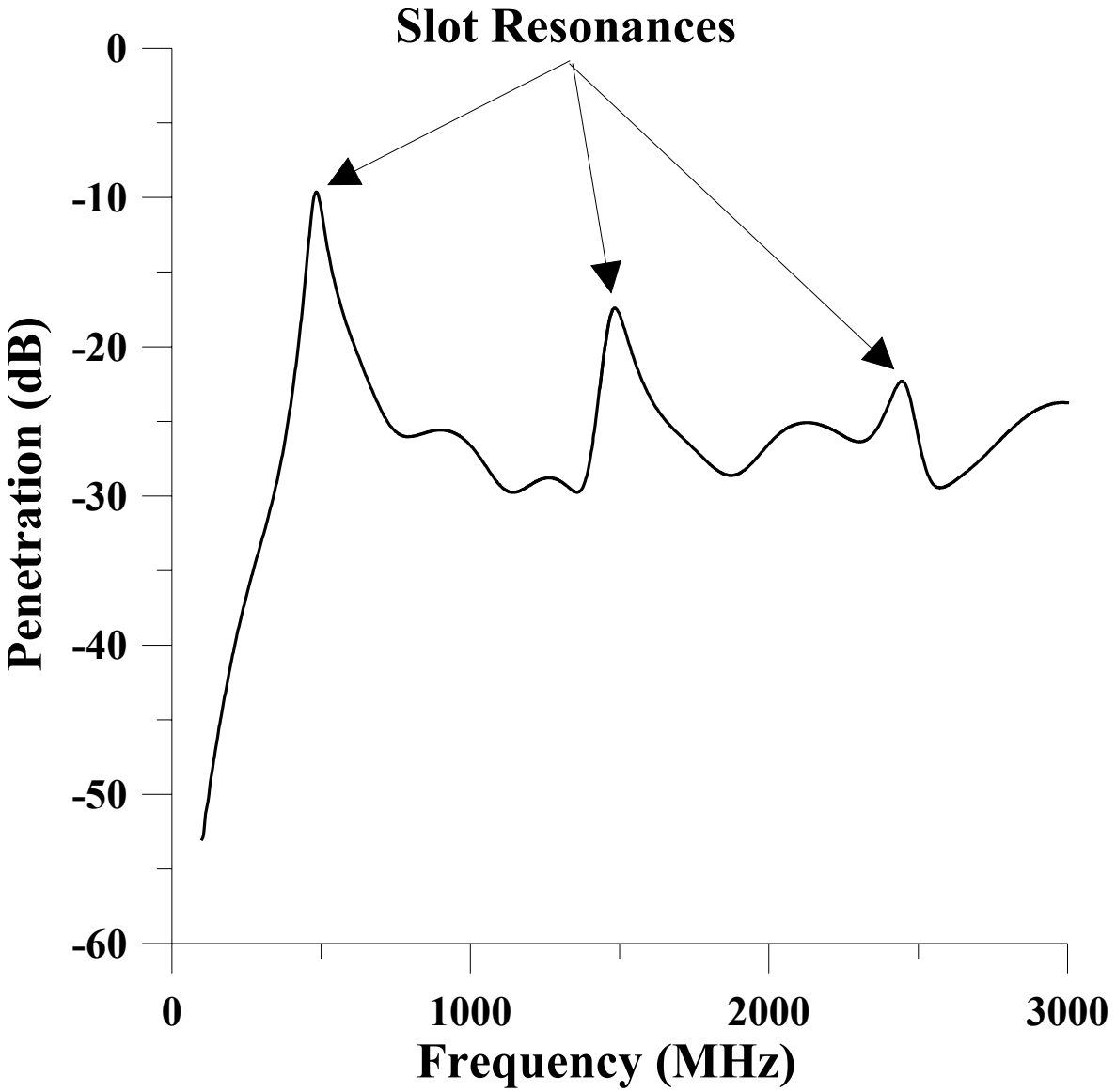

Figure 7. Normalized penetration for a 30 cm x 0.1 cm slot embedded in a perfectly conducting ground plane.

a.

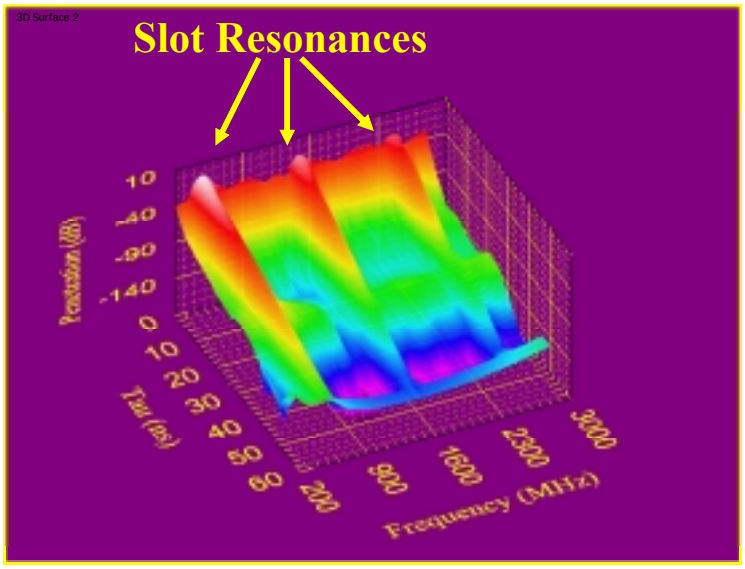

b.

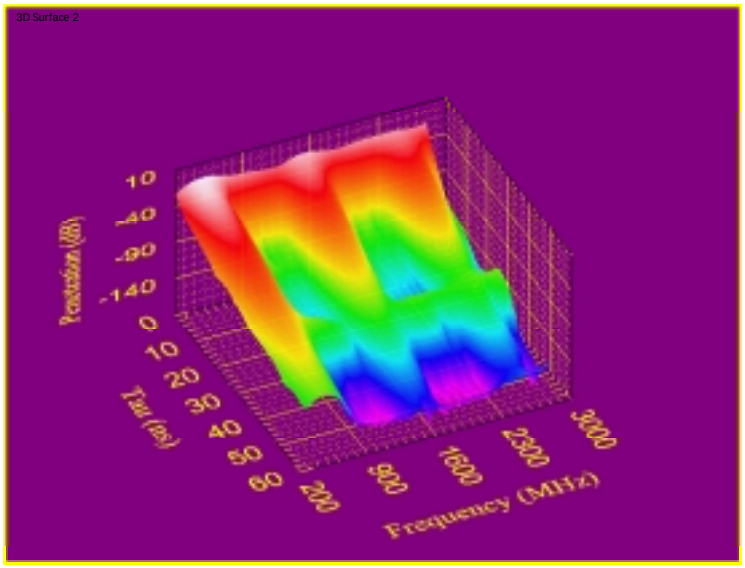

c.

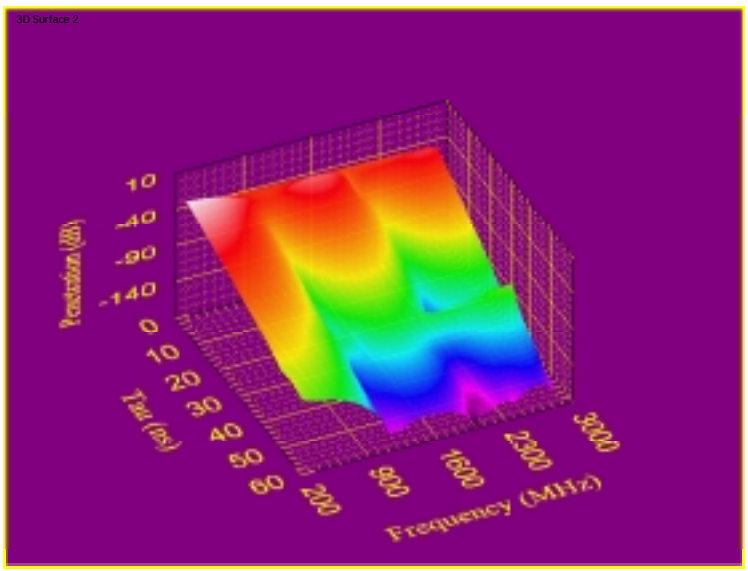

Figure 8. JTFA analysis of the slot waveforms, **a.** 20 ns duration Kaiser-Bessel window with β=3.0, **b.** 10 ns duration Kaiser-Bessel window with β=3.0, **c.** 5 ns duration Kaiser-Bessel window with β=3.0.

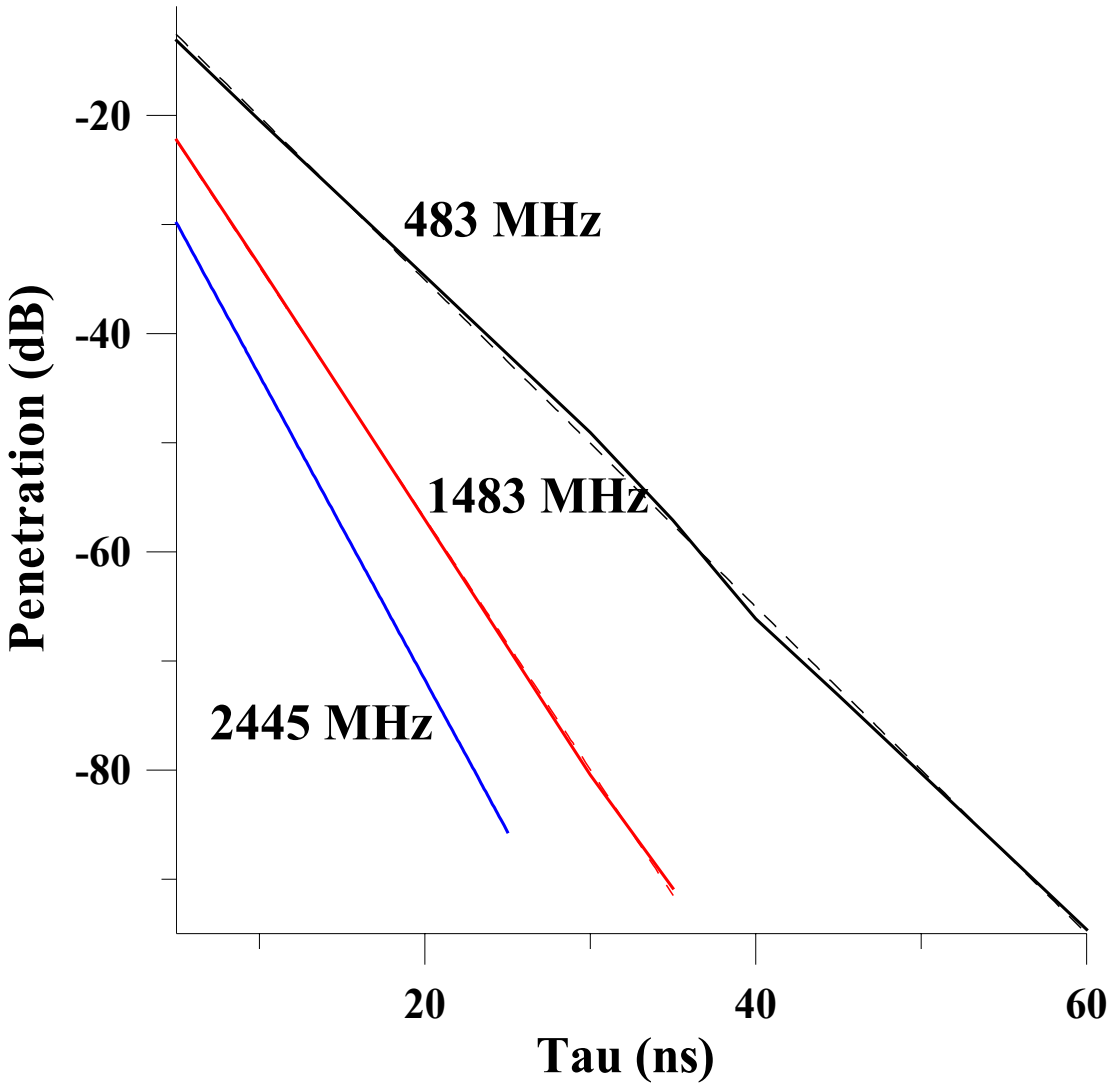

Figure 9. Slot decay characteristics obtained at the resonant peaks using a 10 ns duration Kaiser-Bessel window with β=3.0.

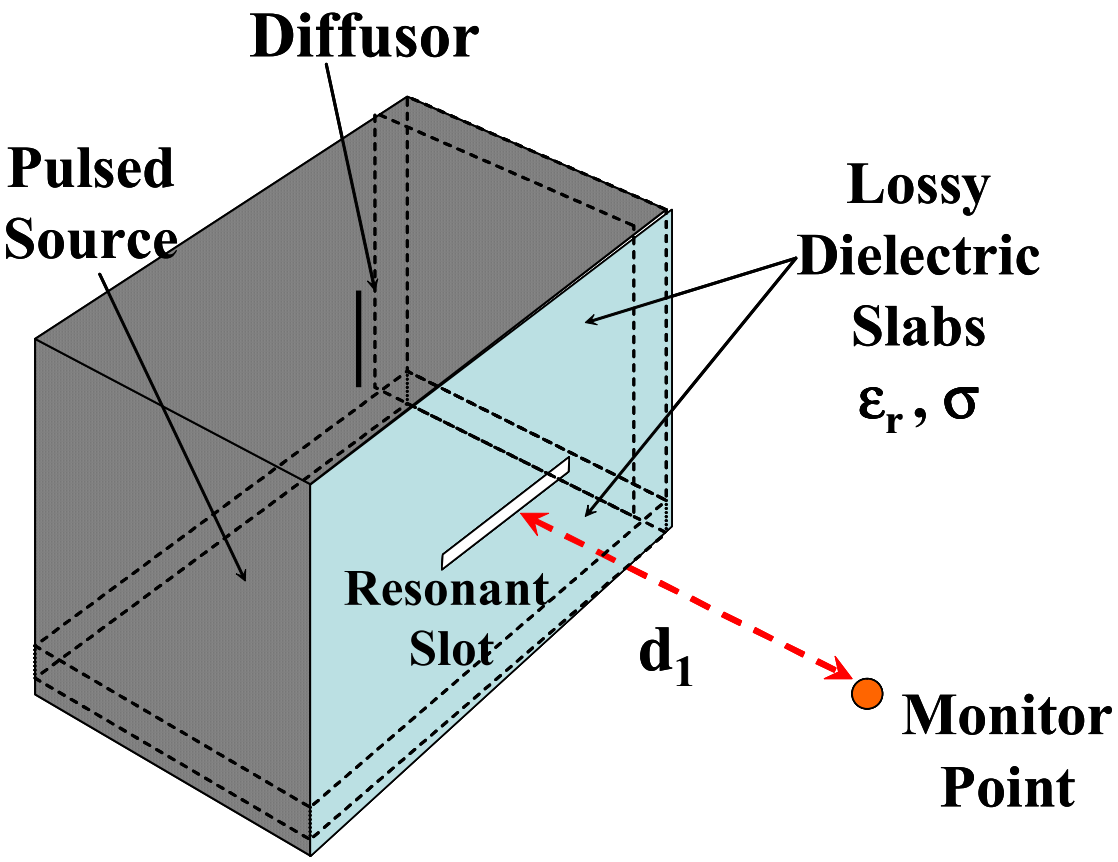

Figure 10. A 1.03 m x 0.93 m x 73 m metal box with a 0.3 m x 0.001 m resonant slot embedded in the face. Two interior box walls are loaded with lossy dielectric slabs with a variable conductance σ and ε_r=1.0. The monitor point is positioned d_1=6.0 m from the center of the slot.

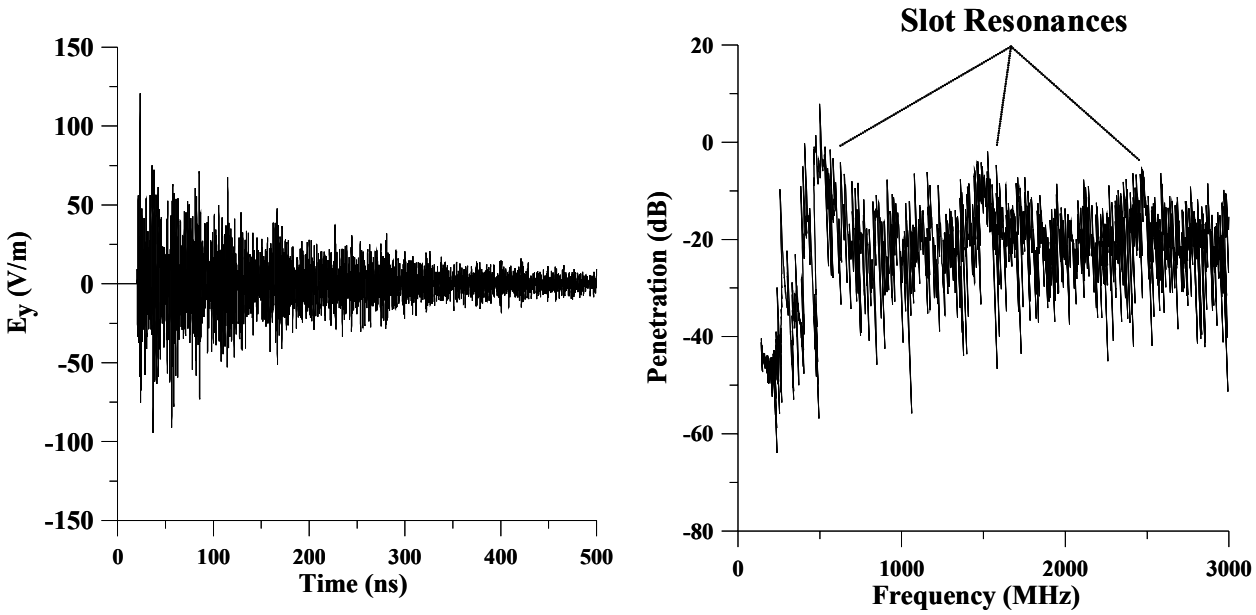

Figure 11. Time domain box electric field waveform and associated penetration spectrum obtained at a monitor point 6.0 m from the center of a 30 cm x 0.1 cm slot embedded in a highly conducting metal box. The lossy slabs each have a conductance σ = 250 S/m. Note the peaks in the penetration in the neighborhood of the slot resonances.

a.

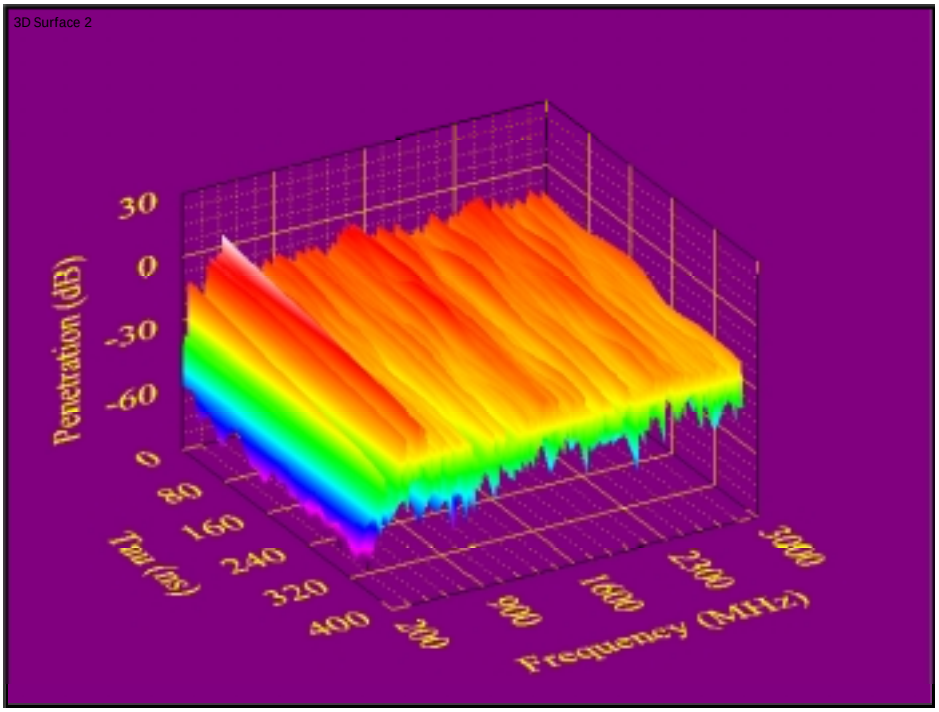

b.

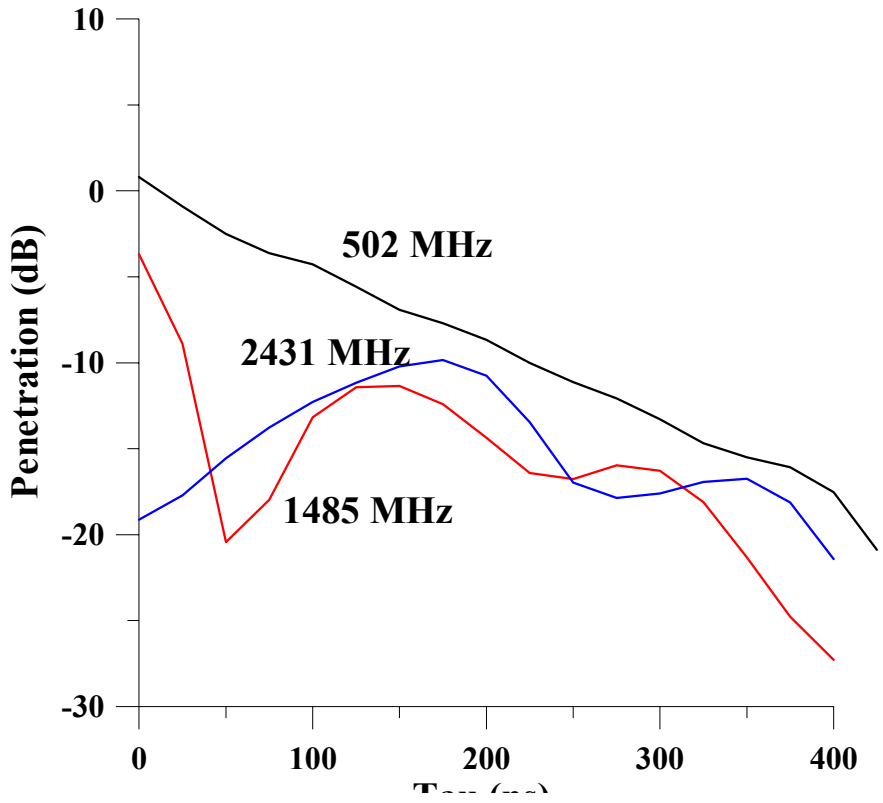

Figure 12 **a.** Joint time-frequency analysis of the box/slot combination with σ = 250 S/m. A 200ns wide Kaiser-Bessel window (β=2.0) is used. Note the complex structure of the penetration spectrum due to the box cavity modes, **b.** selected spectral decay components—note the erratic decay caused by interference between closely spaced box cavity modes.

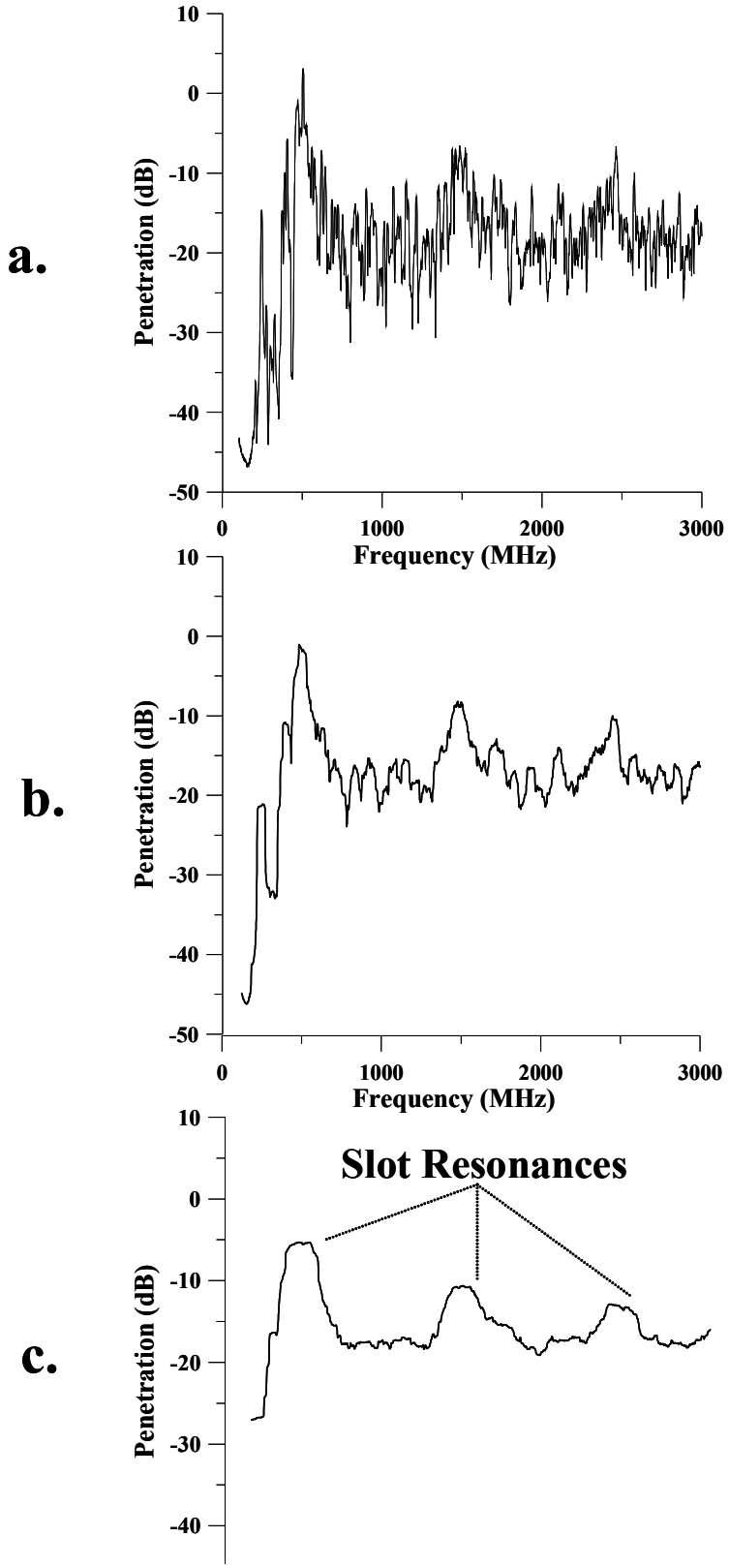

Figure 13. Impact of frequency averaging on the of box/slot structure penetration amplitude spectrum using a 200ns wide Kaiser-Bessel window (β=2.0), **a.** 50 MHz averaging bandwidth, **b.** 100 MHz averaging bandwidth, **c.** 200 MHz averaging bandwidth. Note how the slot resonances become more visible as the averaging bandwidth is increased.

a.

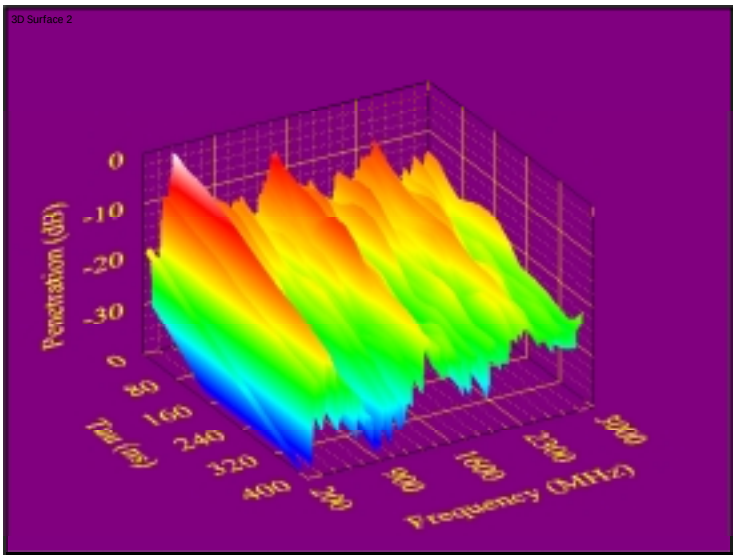

b.

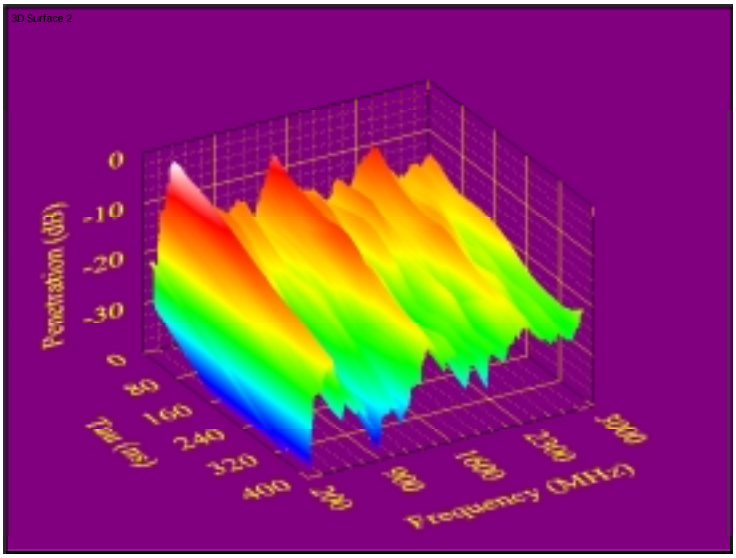

c.

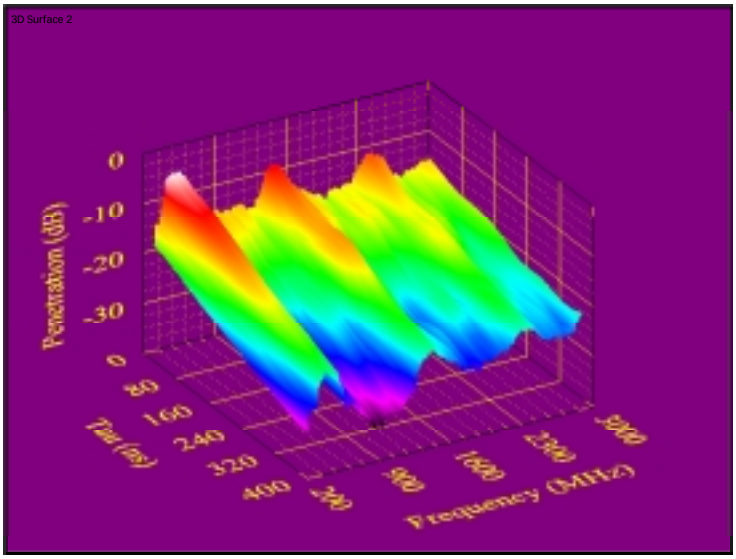

Figure 14. Impact of frequency averaging on the JTFA of box/slot structure penetration, **a.** 50 MHz, **b.** 100 MHz, **c.** 200 MHz. 200ns wide Kaiser-Bessel window (β=2.0) is used. Note how the slot resonances become more visible as the averaging bandwidth is increased.

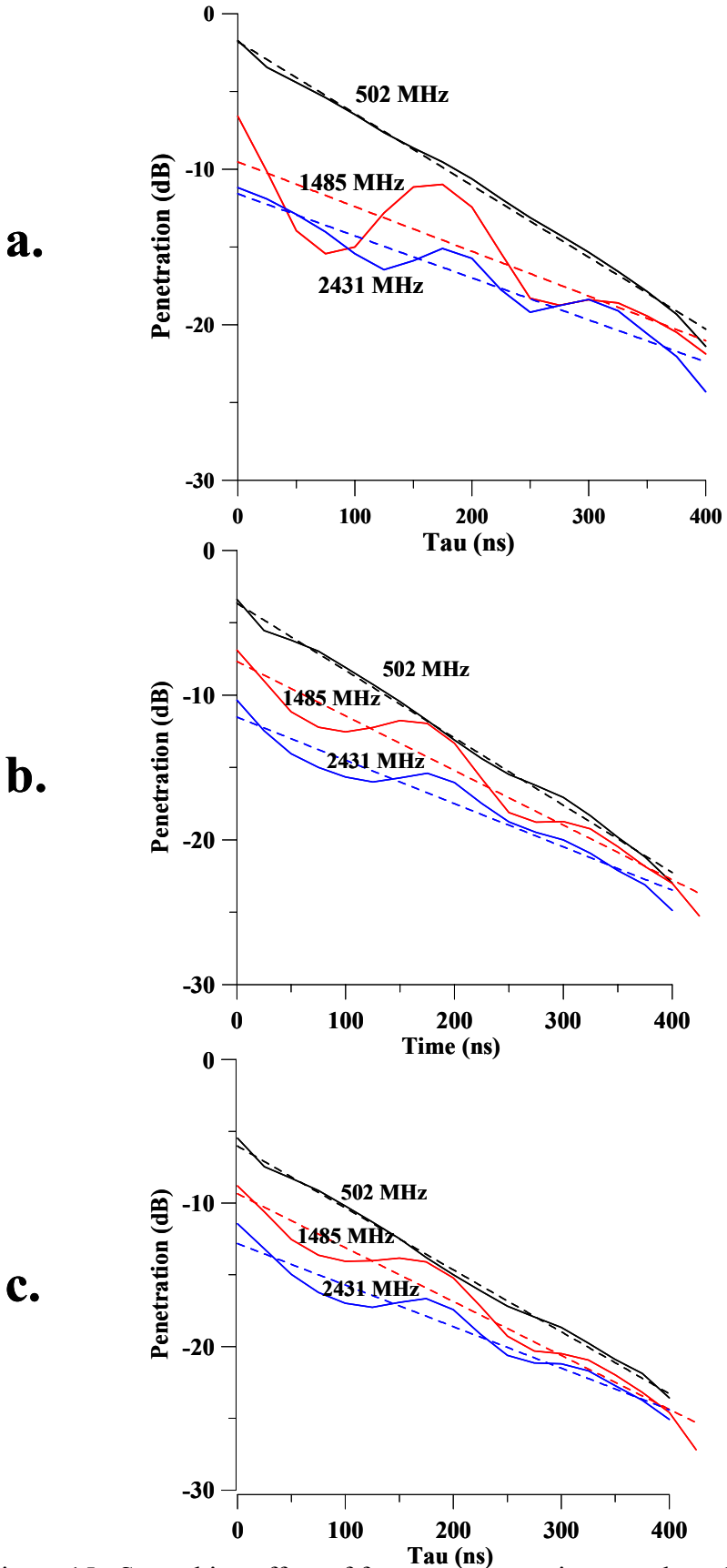

Figure 15. Smoothing effect of frequency averaging on selected frequency components, **a.** 50 MHz averaging bandwidth, **b.** 100 MHz averaging bandwidth, **c.** 200 MHz averaging bandwidth. Note how increased bandwidths reduces interferences effects between adjacent modes and accentuates the exponential decay with only minor variations in the slope of the extracted decay.

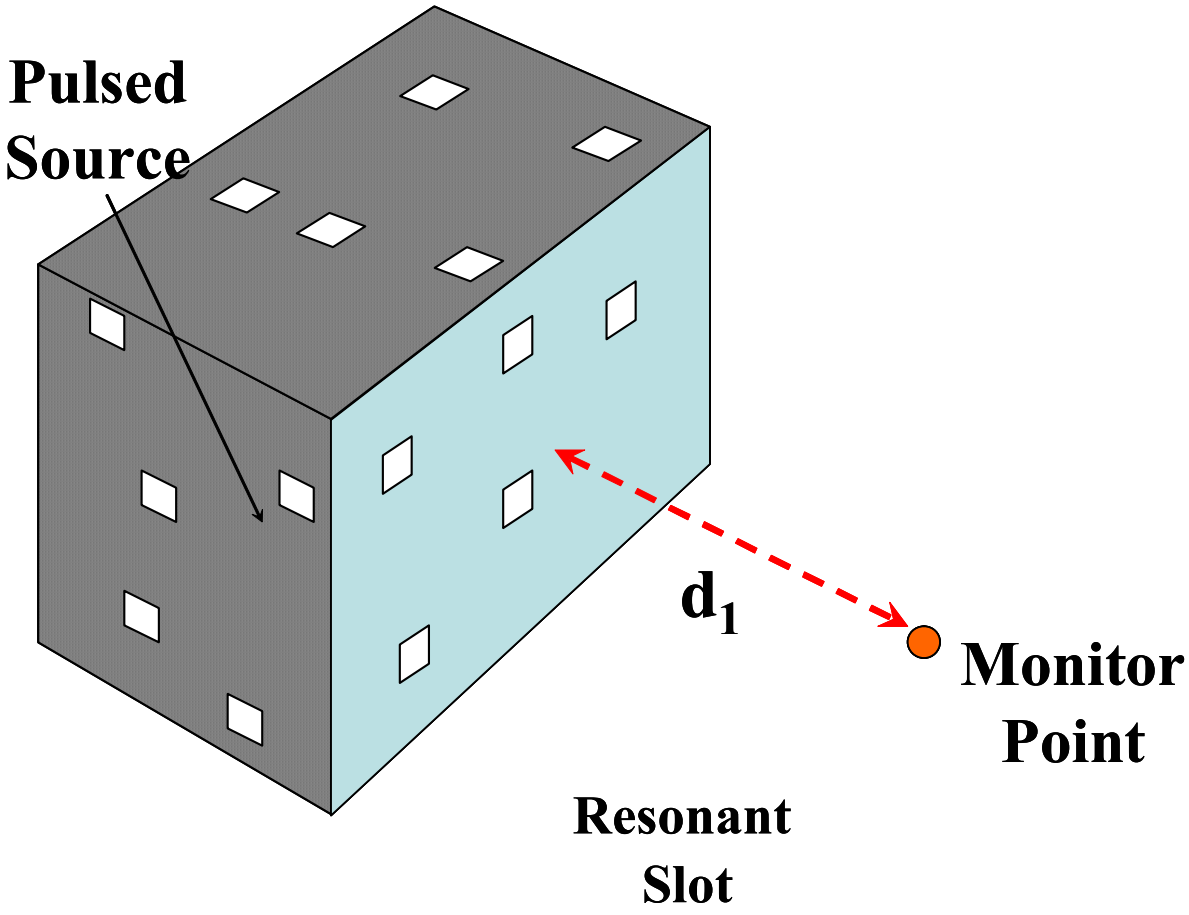

Figure 16. A 1.03 m x 0.93 m x 73 m metal box with five 4 cm x 4 cm apertures embedded in each face. The monitor point is positioned d_1=6.0 m from the center of the front face. The interior of the box is unloaded, and the only loss is due to radiation from the apertures.

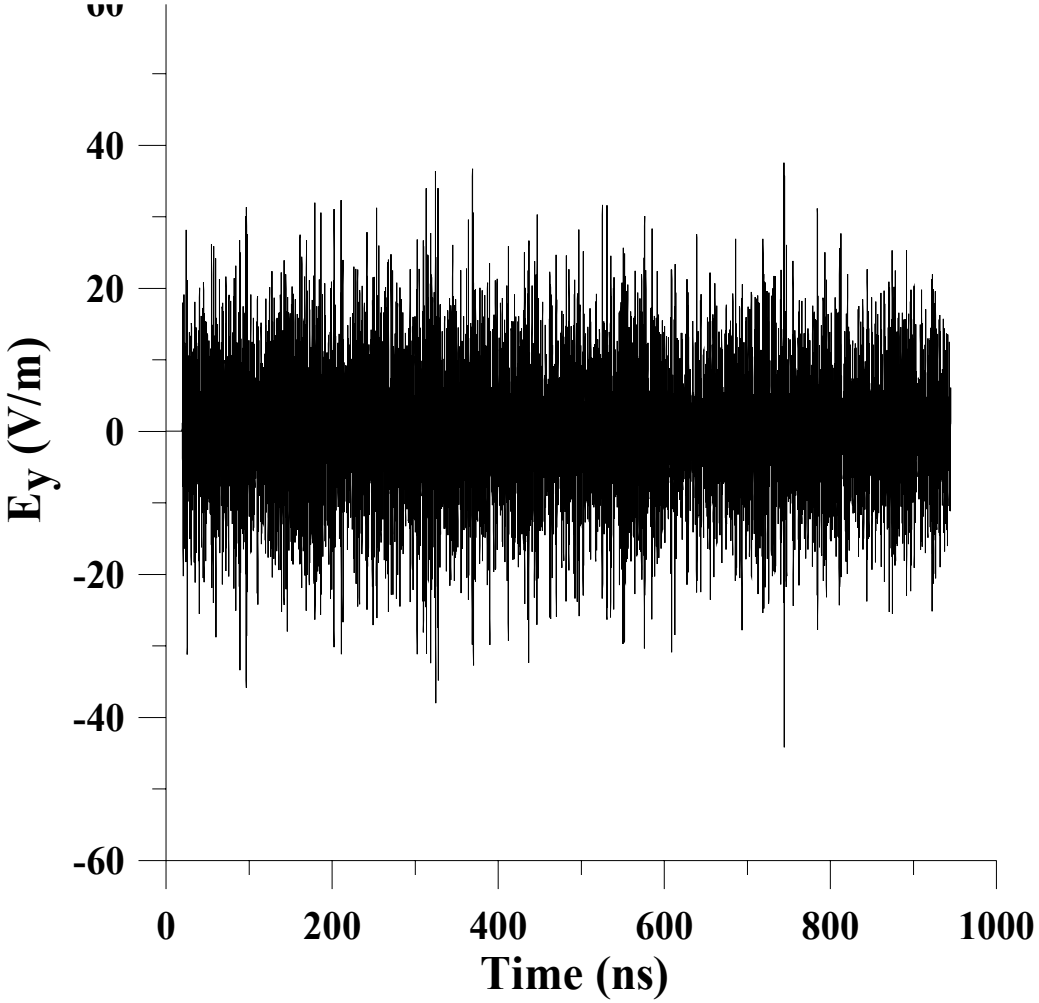

Figure 17. Time domain box waveform obtained at the monitor point. Note that there is no appreciable decay due to small aperture radiation efficiency.

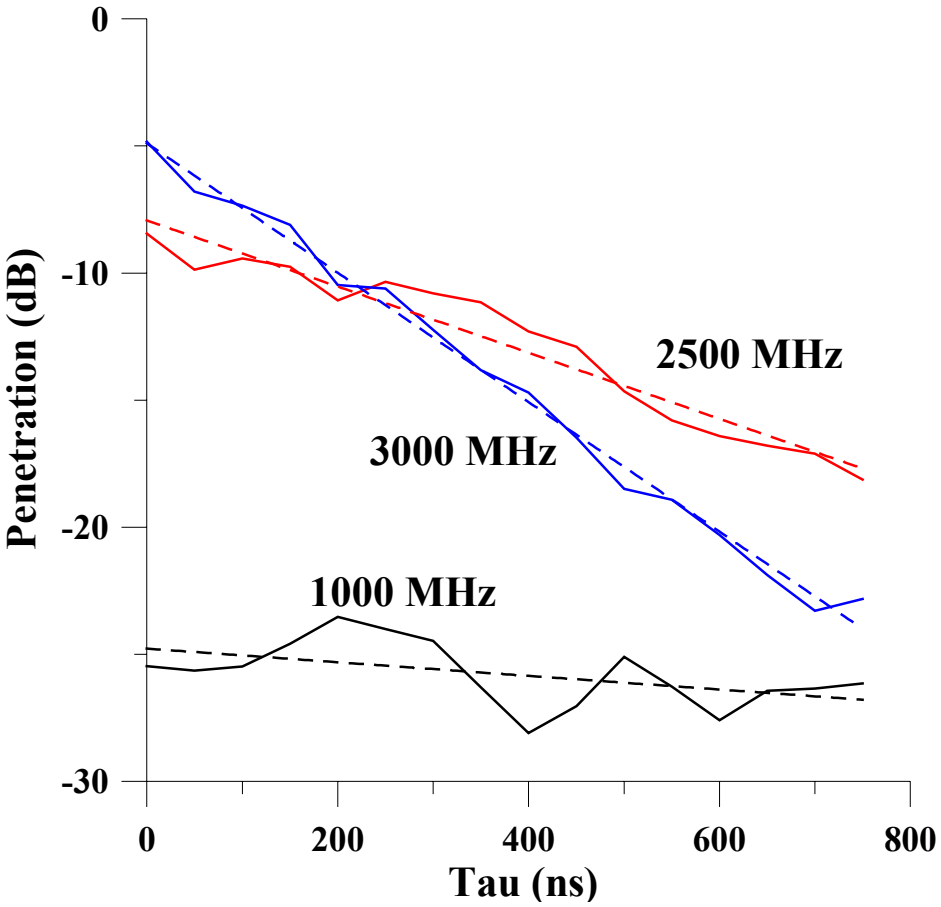

Figure 18. JTFA analysis of the box loaded with thirty 4 cm x 4 cm slots. Note the increased decay rates at the higher frequencies due to increased radiation efficiency.

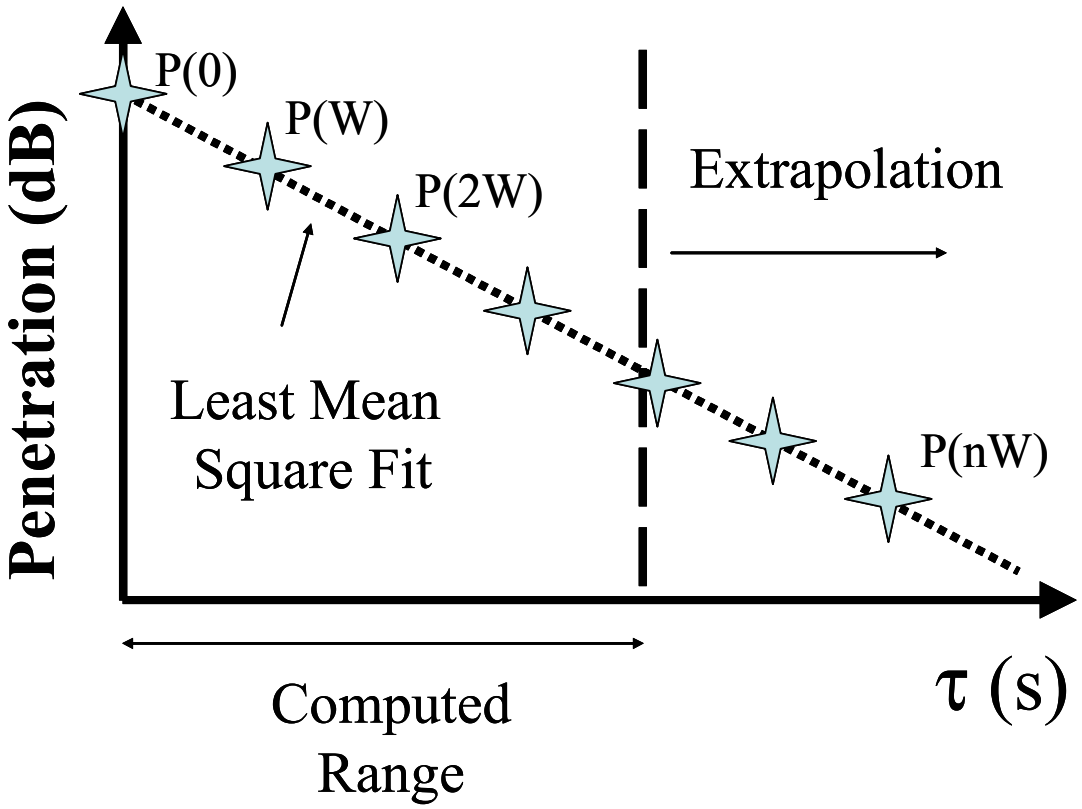

Figure 19. Computing total penetration from a least-squares fit. Samples are taken at an equal interval W, corresponding to the window width selected for the original JTFA analysis. The samples are then summed to obtain total penetration.